Structural Engineering and Mechanics, Vol. 22, No. 1 (2006) 1-16
DOI: http://dx.doi.org/10.12989/sem.2006.22.1.001

Virtual boundary element–equivalent collocation method for the plane magnetoelectroelastic solids

Wei-An Yao† and Xiao-Chuan Li‡

State Key Laboratory of Structural Analysis for Institute Equipment, Dalian University of Technology, Dalian, 116023, P. R. China

Gui-Rong Yu‡†

Department of Science, Shenyang Institute of Aeronautical Engineering, Shenyang, 110034, P. R. China

(Received February 3, 2005, Accepted September 22, 2005)

Abstract. This paper presents a virtual boundary element-equivalent collocation method (VBEM) for the plane magnetoelectroelastic solids, which is based on the fundamental solutions of the plane magnetoelectroelastic solids and the basic idea of the virtual boundary element method for elasticity. Besides all the advantages of the conventional boundary element method (BEM) over domain discretization methods, this method avoids the computation of singular integral on the boundary by introducing the virtual boundary. In the end, several numerical examples are performed to demonstrate the performance of this method, and the results show that they agree well with the exact solutions. So the method is one of the efficient numerical methods used to analyze megnatoelectroelastic solids.

Key words: magnetoelectroelastic solids; plane problem; virtual boundary element; fundamental solution; collocation method.

1. Introduction

Because of possessing mechanical, electric and magnetic field coupling capacity, the magnetoelectroelastic solids become a kind of new functional material, and show better foreground in many high-tech areas. Over the years, a large amount of studies have been done in mechanics, materials science and physics fields (Liu *et al.* 2001, Wang and Shen 2002, 2003, Pan and Heyliger 2003, Wang and Mai 2004, Jiang and Ding 2004) and it has become a new cross subject. Due to multi-fields coupling, the magnetoelectroelastic solids problem is solved more difficultly than elasticity one.

As for numerical solution of magnetoelectroelastic solids problem, to the author's knowledge, a little of work has been done. Buchanan (2004) used the finite element method to analyze the

† Professor, Corresponding author, E-mail: ywa@dlut.edu.cn
‡ Doctoral Candidate, E-mail: li_xiaochuan@tom.com
‡† Associate Professor, E-mail: yugr2004@yahoo.com

vibration problem of infinite plates. Garcia Lage *et al.* (2004) presented a partial mixed layer wise finite element model for adaptive plate structures. Ding and Jiang (2003, 2004) obtained the fundamental solution and the boundary integral formulation of 2D and 3D problems in magnetoelectroelastic solids, and utilized the boundary element method (BEM) to analyze them.

However, the classical boundary element methods (BEM) all inevitably come across the computation of singular integral, which are caused when the source point lies in the integral element or closes to the integral element. In order to solve this problem, Sun *et al.* (1997, 1999) developed the virtual boundary element method (VBEM) for elasticity. The method skillfully avoids the computation of singular integral, and the numerical results with it show higher precision. Recently, Yao and Wang (2005) successfully applied VBEM to analyze the mechanical behavior of the piezoelectric media. The method merely uses collocations technology on real and virtual boundary, so it is a kind of boundary-type meshless method, simultaneity, is integrate-free one. In resent years, as more researchers pay attention to the meshless method, many achievements have obtained in the area. As for the boundary-type meshless methods, Mukherjee *et al.* (1997, 2000) proposed the boundary node method (BNM) combined of moving least squares (MLS) interpolation with boundary integral equations (BIE) and solved three-dimensional linear elasticity problems; Chen (2002) presented the boundary particle method (BPM) based on the multiple reciprocity principle and applied either high-order nonsingular general solutions or singular fundamental solutions as the radial basis function and gave numerical investigations on Helmholtz problems and convection-diffusion problems. By far, the VBEM has not been used to analyze the magnetoelectroelastic solid problems yet.

Based on the basic idea of VBEM for elasticity and the fundamental solutions presented by Ding and Jiang (2004), this paper presents the virtual boundary element-equavilent collocation method for the plane problem of magnetoelectroelastic solids. Finally, several numerical examples are employed to verify the performance of the method presented in this paper, and the numerical results show that they agree well with the exact solution available. So the virtual boundary element is very efficient numerical method to analyze the plane magnetoelectroelastic solids.

2. Functional equations and boundary conditions

The transversely isotropic magnetoelectroelastic solids are studied here, where the z-axis is the polar direction. If geometry size, load etc. in y direction satisfy the given condition, the problem can be simplified as a plane problem in the xoz plane. The functional equations of the plane problem are as follows:

(1) Governing equations:

$$\begin{cases} \dfrac{\partial \sigma_x}{\partial x} + \dfrac{\partial \tau_{xz}}{\partial z} = f_x, & \dfrac{\partial \tau_{xz}}{\partial x} + \dfrac{\partial \sigma_z}{\partial z} = f_z \\ \dfrac{\partial D_x}{\partial x} + \dfrac{\partial D_z}{\partial z} = \rho, & \dfrac{\partial B_x}{\partial x} + \dfrac{\partial B_z}{\partial z} = 0 \end{cases} \tag{1}$$

(2) Gradient equations:

$$\begin{cases} \varepsilon_x = \dfrac{\partial u}{\partial x}, \quad \varepsilon_z = \dfrac{\partial w}{\partial z}, \quad \gamma_{xz} = \dfrac{\partial w}{\partial x} + \dfrac{\partial u}{\partial z} \\ E_x = -\dfrac{\partial \Phi}{\partial x}, \quad E_z = -\dfrac{\partial \Phi}{\partial z} \\ H_x = -\dfrac{\partial \Psi}{\partial x}, \quad H_z = -\dfrac{\partial \Psi}{\partial z} \end{cases} \tag{2}$$

(3) Constitutive equations:

$$\begin{cases} \sigma_x = c_{11}\varepsilon_x + c_{13}\varepsilon_z - e_{31}E_z - q_{31}H_z \\ \sigma_z = c_{13}\varepsilon_x + c_{33}\varepsilon_z - e_{33}E_z - q_{33}H_z \\ \tau_{xz} = c_{44}\gamma_{xz} - e_{15}E_x - q_{15}H_x \\ D_x = e_{15}\gamma_{xz} + \kappa_{11}E_x + \alpha_{11}H_x \\ D_z = e_{31}\varepsilon_x + e_{33}\varepsilon_z + \kappa_{33}E_z + \alpha_{33}H_z \\ B_x = q_{15}\gamma_{xz} + \alpha_{11}E_x + \mu_{11}H_x \\ B_z = q_{31}\varepsilon_x + q_{33}\varepsilon_z + \alpha_{33}E_z + \mu_{33}H_z \end{cases} \tag{3}$$

where u, w are displacement components in the x, z direction, respectively; σ_x, σ_z and τ_{xz} are stress components, respectively; D_x, D_z and Φ are electric displacement components and electric potential, respectively; B_x, B_z and Ψ are magnetic induction components and magnetic potential, respectively; f_x, f_z and ρ are body force components and density of free charges in region V, respectively; c_{ij}, κ_{ij} and μ_{ij} are elastic modus, dielectric constant and magnetic constants, respectively; e_{ij}, q_{ij} and α_{ij} are piezoelectric, piezomagnetic and electromagnetic constants, respectively.

And the boundary conditions on Γ are expressed as:

(1) mechanical boundary conditions

$$u = \bar{u}, \quad w = \bar{w} \qquad \text{on} \quad \Gamma_u \tag{4}$$

$$\sigma_x n_x + \tau_{xz} n_z = \bar{t}_x, \quad \tau_{xz} n_x + \sigma_z n_z = \bar{t}_z \quad \text{on} \quad \Gamma_t \tag{5}$$

where n_i are the direction cosines of the outward normal on the boundary Γ.

(2) electrical boundary conditions

$$D_x n_x + D_z n_z = \bar{g} \quad \text{on} \quad \Gamma_g \tag{6}$$

$$\Phi = \bar{\Phi} \qquad \text{on} \quad \Gamma_\phi \tag{7}$$

(3) magnetic boundary conditions

$$B_x n_x + B_z n_z = \bar{m} \quad \text{on} \quad \Gamma_m \tag{8}$$

$$\Psi = \overline{\Psi} \quad \text{on} \quad \Gamma_{\psi} \tag{9}$$

meanwhile $\Gamma_t + \Gamma_u = \Gamma_g + \Gamma_\phi = \Gamma_m + \Gamma_\psi = \Gamma$, $\Gamma_t \cap \Gamma_u = \Gamma_g \cap \Gamma_\phi = \Gamma_m \cap \Gamma_\psi = 0$.

3. The fundamental solution (Ding and Jiang 2004)

The fundamental solutions to the problem are necessary when VBEM is applied to solve that one. Ding and Jiang (2004) obtained the two-dimensional fundamental solutions for an infinite magetoelectroelastic plane by virtue of the trail-and error method to construct harmonic functions. For sake of convenience, the following notations are introduced:

$U_n(n = 1\sim4)$ are the general displacemen u, w, Φ and Ψ, respectively; $T_n(n = 1\sim7)$ are the general stress σ_x, τ_{xz}, σ_z, D_x, D_z, B_x and B_z, respectively; $U^*_{nj}(X, X_k)$ and $T^*_{nj}(X, X_k)$ are, respectively, the general displacements, u^*_j, w^*_j, Φ^*_j and Ψ^*_j, and the general stress, σ^*_{xj}, τ^*_{xzj}, σ^*_{zj}, D^*_{xj}, D^*_{zj}, B^*_{xj} and B^*_{zj}, at field point $X(x, z)$ due to x- and z-direction unit point force ($j = 1, 2$), unit point charge ($j = 3$) and unit point current ($j = 4$) acting at a source point $X_k(\xi, \eta)$.

As showed by Ding and Jiang (2004), the fundamental solutions to the problem of magetoelectroelastic plane are as follows:

$$\begin{cases} U^*_{11} = \sum_{i=1}^{4} \lambda_i \ln R_i \\ U^*_{12} = -\sum_{i=1}^{4} \alpha_i \arctan\dfrac{x}{z_i} \\ U^*_{13} = -\sum_{i=1}^{4} \beta_i \arctan\dfrac{x}{z_i} \\ U^*_{14} = -\sum_{i=1}^{4} \gamma_i \arctan\dfrac{x}{z_i} \end{cases} \tag{10}$$

$$\begin{cases} U^*_{n1} = \sum_{i=1}^{4} s_i k_{mi} \lambda_i \arctan\dfrac{x}{z_i} \\ U^*_{n2} = \sum_{i=1}^{4} s_i k_{mi} \alpha_i \ln R_i \\ U^*_{n3} = \sum_{i=1}^{4} s_i k_{mi} \beta_i \ln R_i \\ U^*_{n4} = \sum_{i=1}^{4} s_i k_{mi} \gamma_i \ln R_i \end{cases} \qquad m = 1, 2, 3;\ n = m + 1 \tag{11}$$

$$\begin{cases} T_{11}^{*} = -\sum_{i=1}^{4} \omega_{4i} \dfrac{\lambda_i x}{R_i^2} \\ T_{12}^{*} = \sum_{i=1}^{4} \omega_{4i} \dfrac{\alpha_i z_i}{R_i^2} \\ T_{13}^{*} = \sum_{i=1}^{4} \omega_{4i} \dfrac{\beta_i z_i}{R_i^2} \\ T_{14}^{*} = \sum_{i=1}^{4} \omega_{4i} \dfrac{\gamma_i z_i}{R_i^2} \end{cases} \tag{12}$$

$$\begin{cases} T_{n1}^{*} = \sum_{i=1}^{4} s_i \omega_{mi} \dfrac{\lambda_i z_i}{R_i^2} \\ T_{n2}^{*} = \sum_{i=1}^{4} s_i \omega_{mi} \dfrac{\alpha_i x}{R_i^2} \\ T_{n3}^{*} = \sum_{i=1}^{4} s_i \omega_{mi} \dfrac{\beta_i x}{R_i^2} \\ T_{n4}^{*} = \sum_{i=1}^{4} s_i \omega_{mi} \dfrac{\gamma_i x}{R_i^2} \end{cases} \qquad m = 1, 2, 3;\ n = 2m \tag{13}$$

$$\begin{cases} T_{n1}^{*} = -\sum_{i=1}^{4} \omega_{mi} \dfrac{\lambda_i x}{R_i^2} \\ T_{n2}^{*} = \sum_{i=1}^{4} \omega_{mi} \dfrac{\alpha_i z_i}{R_i^2} \\ T_{n3}^{*} = \sum_{i=1}^{4} \omega_{mi} \dfrac{\beta_i z_i}{R_i^2} \\ T_{n4}^{*} = \sum_{i=1}^{4} \omega_{mi} \dfrac{\gamma_i z_i}{R_i^2} \end{cases} \qquad m = 1, 2, 3;\ n = 2m + 1 \tag{14}$$

where $z_i = s_i z$ and $R_i = \sqrt{x^2 + z_i^2}$, in addition s_i, k_{mi}, ω_{mi}, λ_i, α_i, β_i and γ_i all are relate to material constants of magnetoelectroelastic solid, and their expression are gave by Ding and Jiang (2004).

4. Virtual boundary element–equivalent collocation method

Above all, extend the region V to the infinite region, in which a virtual boundary Γ' is selected to

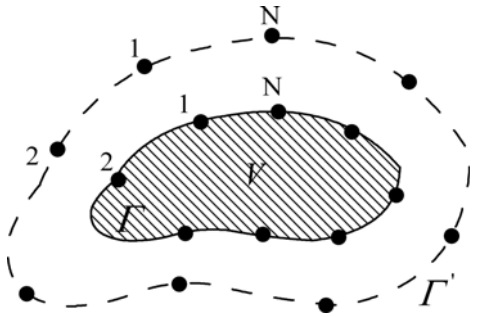

Fig. 1 The real boundary and its corresponding virtual boundary

be similarity with real boundary, as shown in Fig. 1. The similarity ratio between the virtual boundary and the real one is discussed in next section in detail. Then discretize the real boundary Γ and the virtual boundary Γ', and choose N points $X_{\xi k}$, $X_{\eta k}$ $(k = 1, 2, \ldots, N)$ on them, respectively. Suppose there are general unknown virtual loads $(a_{k1}, a_{k2}, a_{k3}, a_{k4})$ $(k = 1, 2, \ldots, N)$ on the virtual boundary, where a_{k1}, a_{k2}, a_{k3} and a_{k4} denote x- and z-direction point force, point charge and point current at the point $X_{\eta k}$ $(k = 1, 2, \ldots, N)$, respectively.

Assume that, in region V, there are M points $X_{dm}(m = 1, 2, \ldots, M)$, where subjected to x- and z-direction point force and point charge d_{m1}, d_{m2} and d_{m3}, respectively. According to the fundamental solutions for plane magnetoelectroelastic solids problem and superposition principle, the expressions of the displacements, electric potential, magnetic potential, stress, electric displacements and magnetic induction at random point X in region V are as follows:

$$U_n(X) = \sum_{k=1}^{N}\sum_{j=1}^{4} U_{nj}^{*}(X, X_{\eta k})a_{kj} + \sum_{m=1}^{M}\sum_{j=1}^{3} U_{nj}^{*}(X, X_{dm})d_{mj} \qquad (n = 1\sim4) \tag{15}$$

$$T_n(X) = \sum_{k=1}^{N}\sum_{j=1}^{4} T_{nj}^{*}(X, X_{\eta k})a_{kj} + \sum_{m=1}^{M}\sum_{j=1}^{3} T_{nj}^{*}(X, X_{dm})d_{mj} \qquad (n = 1\sim7) \tag{16}$$

Eq. (15) and Eq. (16) satisfy all the differential Eqs. (1)-(3) in the domain V, but include $4N$ unknown values $a_{kj}(k = 1, 2, \ldots, N; j = 1, 2, 3, 4)$. Further, let Eq. (15) and Eq. (16) satisfy given boundary conditions at points $X_{\xi m}(m = 1, 2, \ldots, N)$, so $4N$ algebra equations can be obtained in matrix form

$$\mathbf{HA} = \mathbf{Y} \tag{17}$$

where $\mathbf{H}$ represents an influence matrix of dimensions $4N \times 4N$, $\mathbf{A} = [a_{11}\ a_{12}\ a_{13}\ a_{14} \cdots\ a_{N1}\ a_{N2}\ a_{N3}\ a_{N4}]^T$ is a undetermined vector of dimension $4N$, and $\mathbf{Y}$ stands for a $4N$ dimensional vector which is formed according to the given boundary conditions at points $X_{\xi m}(m = 1, 2, \ldots, N)$ on the real boundary.

Solve above equations, and all the unknown virtual loads a_{kj} can be achieved. Finally, substitute obtained virtual loads a_{kj} into Eq. (15) and Eq. (16), numerical solutions of the displacement, electric potential, magnetic potential, stress, electric displacement and magnetic induction *et al.* at random points in domain V are obtained.

5. Numerical examples

In the following the numerical examples, the composite materials $BaTiO_3$-$CoFe_2O_4$ are specified, which material constants are given by Ding and Jiang (2004) as

$$c_{11} = 16.6, \quad c_{12} = 7.7, \quad c_{13} = 7.8, \quad c_{33} = 16.2, \quad c_{44} = 4.3, \quad c_{66} = 4.45 \quad (\times 10^{10}\ \mathrm{N/m^2})$$

$$e_{31} = -4.4, \quad e_{33} = 18.6, \quad e_{15} = 11.6 \quad (\mathrm{C/m^2})$$

$$d_{31} = 580.3, \quad d_{33} = 699.7, \quad d_{15} = 550 \quad (\mathrm{N/Am})$$

$$\varepsilon_{11} = 1.12, \quad \varepsilon_{33} = 1.26 \quad (\times 10^{-8}\ \mathrm{C/Vm})$$

$$g_{11} = 5.0, \quad g_{33} = 3.0 \quad (\times 10^{-12}\ \mathrm{Ns^2/C^2})$$

$$\mu_{11} = 5.0, \quad \mu_{33} = 10.0 \quad (\times 10^{-6}\ \mathrm{Ns/VC})$$

Example 1: Consider a magnetoelectroelastic rectangle domain, as shown in Fig. 2, under uniform axial tension, electrical displacement or magnetic induction, respectively. The dimension of the rectangle is $a = 3$ cm, $h = 10$ cm. In terms of its symmetry, only the quarter part of the rectangle domain in top right corner is studied. The problem is treated as a plane-strain one and the boundary conditions are

$$u = \tau_{xz} = D_x = B_x = 0, \qquad \text{at } x = 0 \tag{18}$$

$$\sigma_x = \tau_{xz} = D_x = B_x = 0, \qquad \text{at } x = a \tag{19}$$

$$\tau_{xz} = w = \Phi = \Psi = 0, \qquad \text{at } z = 0 \tag{20}$$

and the boundary condition at $z = h$ is

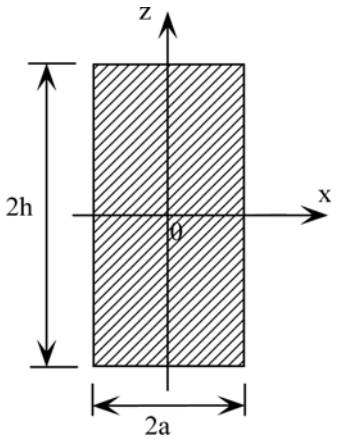

Fig. 2 The rectangle domain problem for the megnatoelectroelastic solid

(a) under uniform tension

$$\sigma_z = 10\ \mathrm{N/m^2},\quad \tau_{xz} = D_z = B_z = 0 \quad \text{at } z = h \tag{21}$$

(b) under uniform electric displacement

$$D_z = 10^{-9}\ \mathrm{C/m^2},\quad \sigma_z = \tau_{xz} = B_z = 0 \quad \text{at } z = h \tag{22}$$

(c) under uniform magnetic induction

$$B_z = 10^{-7}\ \mathrm{N/Am},\quad \sigma_z = \tau_{xz} = D_z = 0 \quad \text{at } z = h \tag{23}$$

In the calculation, set the ratio between the virtual boundary and the real boundary as 2.5, take total 40 collocations on the virtual boundary and the real boundary, respectively. The numerical results at the point (a, h) are given in Table 1, where the values in the parenthesis are the exact ones which are calculated with formulas presented by Ding and Jiang (2004). The results show that the numerical solutions by VBEM have higher accuracy. Table 2 lists the results with different ratio of between virtual boundary and the real boundary under uniform tension, which validates the explanation about scope of ratio by Sun *et al.* (1999).

Table 1 The compassion of the numerical results and exact ones in the rectangle domain problem

Case	u ($\times10^{13}$ m)	w ($\times10^{12}$ m)	Φ ($\times10^{3}$ V)	Ψ ($\times10^{4}$ A)	σ_z (N/m^2)	D_z ($\times10^{9}$ C/m^2)	B_z ($\times10^{7}$ N/Am)
a	–9.49977 (–9.49976)	5.68337 (5.68338)	9.49550 (9.49549)	2.13907 (2.13906)	10.00000 (10.00000)	0.00000 (0.00000)	0.00000 (0.00000)
b	–2.10784 (–2.10785)	0.949553 (0.949549)	–6.28945 (–6.28944)	0.256686 (0.256691)	0.00000 (0.00000)	1.00000 (1.00000)	0.00000 (0.00000)
c	5.07666 (5.07667)	2.13906 (2.13906)	2.56691 (2.56691)	–7.5213 (–7.5213)	0.00000 (0.00000)	0.00000 (0.00000)	1.00000 (1.00000)

Table 2 The σ_z, Φ and ψ at the point (a, h) under simple tension when ratio between the virtual boundary and the real boundary is given different values

Ratio		1.2	1.3	1.5	1.8	2.0	2.5	3.0	3.5	Exact solutions
σ_z (N/m^2)	VBEM	10.4832	10.0254	10.0203	10.0008	9.99990	10.000	10.000	10.000	10.000
	Error (%)	4.832	0.254	0.203	0.008	–0.001	0.000	0.000	0.000	—
Φ ($\times10^{3}$ V)	VBEM	7.02874	9.53179	9.36279	9.49960	9.52025	9.49550	9.49550	9.49549	9.49549
	Error (%)	–25.978	0.382	–1.398	0.043	0.261	0.000	0.000	0.000	—
ψ ($\times10^{4}$ A)	VBEM	5.20744	1.77593	2.34816	2.14990	2.13717	2.13908	2.13908	2.13906	2.13906
	Error (%)	143.445	–16.976	9.775	0.507	–0.088	0.000	0.000	0.000	—

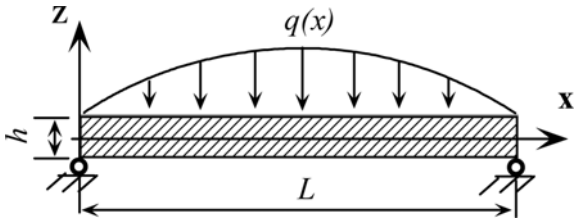

Fig. 3 A simple-supported rectangle beam under distributed load

Example 2: Consider a simply-supported rectangle beam, as shown in Fig. 3, subjected to distributed load on the upper surface, $q(x) = q_0 \sin \pi x/L (q_0 = -10 \text{N/m}^2)$. The dimension of beam is $L = 20$ cm, $h = 2$ cm. The problem is treated as a plane-stress one and the boundary conditions are

$$\sigma_z(x) = q_0 \sin \pi x/L, \quad \tau_{xz} = D_z = B_z = 0, \quad \text{at} \quad z = h/2 \tag{24}$$

$$\sigma_z = \tau_{xz} = D_z = B_z = 0, \quad \text{at} \quad z = -h/2 \tag{25}$$

$$\sigma_x = w = \Phi = \Psi = 0, \quad \text{at} \quad x = 0 \quad \text{or} \quad L \tag{26}$$

In the calculation, set the ratio of the virtual boundary and the real boundary as 2.5, take total 80 collocations on the virtual boundary and the real boundary, respectively. The numerical results at 8 reference points are given in Table 3, where the values in the parenthesis are the exact ones which are calculated with formulas presented by Ding and Jiang (2004).

Table 3 The comparison of the numerical results and exact ones in the simple-supported rectangle beam

Points	w ($\times 10^8$ m)	Φ ($\times 10$ V)	ψ ($\times 10^2$ A)	σ_z (N/m^2)	D_z ($\times 10^{10}$ C/m^2)	B_z ($\times 10^9$ N/Am)	σ_x (N/m^2)
(0.100, 0.000)	–0.2000 (–0.2000)	–0.2314 (–0.2314)	–0.1808 (–0.1808)	–4.9995 (–5.0000)	–0.1107 (–0.1114)	–0.2289 (–0.2282)	0.02748 (0.02818)
(0.125, 0.000)	–0.1847 (–0.1847)	–0.2138 (–0.2138)	–0.1671 (–0.1671)	–4.6193 (–4.6190)	–0.1029 (–0.1029)	–0.2109 (–0.2109)	0.02602 (0.02604)
(0.150, 0.000)	–0.1414 (–0.1414)	–0.1636 (–0.1637)	–0.1279 (–0.1279)	–3.5354 (–3.5153)	–0.07875 (–0.07875)	–0.1614 (–0.1614)	0.01990 (0.01993)
(0.175, 0.000)	–0.07652 (–0.07652)	–0.08856 (–0.08857)	–0.06921 (–0.06921)	–1.9133 (–1.9130)	–0.04269 (–0.04262)	–0.08688 (–0.08734)	0.01074 (0.01078)
(0.100, 0.010)	–0.1993 (–0.1993)	–0.08726 (–0.08728)	–0.2184 (–0.2184)	–10.0000 (–10.0000)	0.0000 (0.0000)	0.0000 (0.0000)	–610.4 (–610.4)
(0.125, 0.010)	–0.1842 (–0.1842)	–0.08062 (–0.08063)	–0.2018 (–0.2018)	–9.2388 (–9.2388)	0.0000 (0.0000)	0.0000 (0.0000)	–564.0 (–564.0)
(0.150, 0.010)	–0.1409 (–0.1409)	–0.06170 (–0.06172)	–0.1544 (–0.1544)	–7.0711 (–7.0711)	0.0000 (0.0000)	0.0000 (0.0000)	–431.6 (–431.6)
(0.175, 0.010)	–0.07628 (–0.07628)	–0.03338 (–0.03340)	–0.08357 (–0.08357)	–3.8268 (–3.8268)	0.0000 (0.0000)	0.0000 (0.0000)	–233.6 (–233.6)

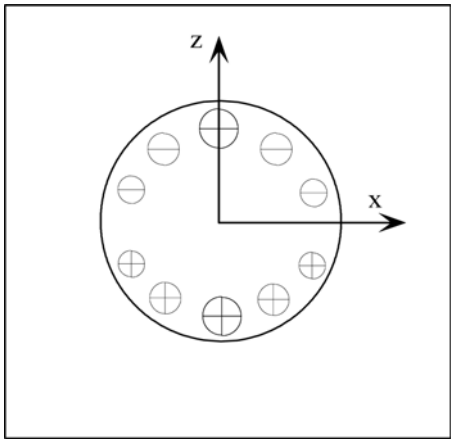

Fig. 4 Infinite plane magnetoelectroelastic solid with a circular hole subjected to a sinusoidal surface charge along the surface of the hole

Example 3: Consider the plane problem of an infinite magnetoelectroelastic material with a circular hole, as shown in Fig. 4, subjected to a sinusoidal surface charge distribution $\omega = -\omega_0 \sin\theta$ ($\omega_0 = 1$C) on the rim of the hole. The radius of the hole is $r_0 = 1$ cm. The problem is treated as a plane-strain one and the boundary conditions are

$$D_r = -\omega, \quad \sigma_r = \tau_{r\theta} = B_r = 0 \quad \text{when} \quad r = r_0 \tag{27}$$

In the calculation, set the ratio of the virtual boundary and the real boundary as 0.7, take total 50 collocations on the virtual boundary and the real boundary, respectively. (Note: Presently no exact solution is found)

Figs. 5-8 show two displacement components, u and w, electric potential Φ and magnetic potential Ψ around the hole subjected to a sinusoidal surface charge distribution.

Figs. 9-11 present the circumferential components of stress σ_θ, electric displacement D_θ and magnetic induction B_θ at the perimeter of the hole. They all reach their maximum value at $\theta = 0^\circ$ and $\theta = 180^\circ$ as indicated in the figures.

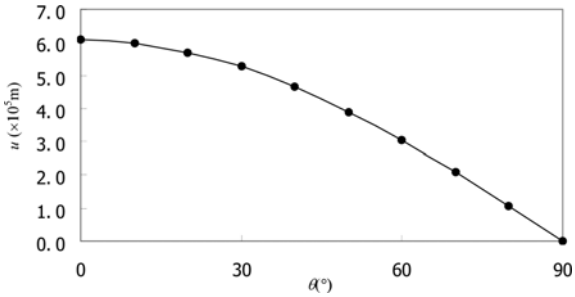

Fig. 5 Distribution of u versus θ on the rim of the circular hole subjected to a sinusoidal surface charge

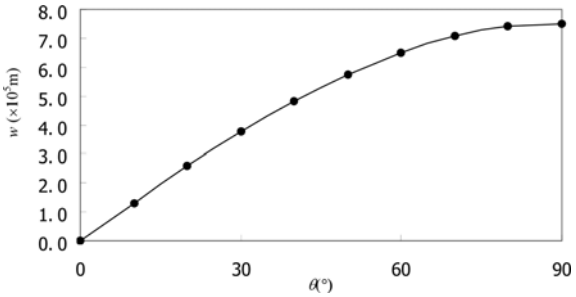

Fig. 6 Distribution of w versus θ on the rim of the circular hole subjected to a sinusoidal surface charge

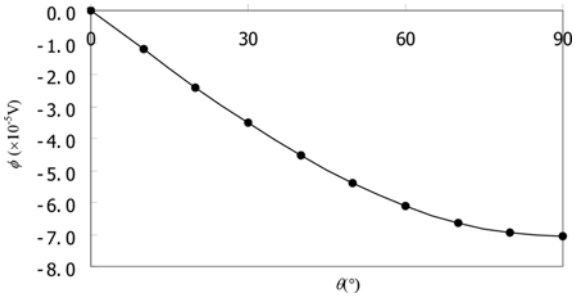

Fig. 7 Distribution of Φ versus θ on the rim of the circular hole subjected to a sinusoidal surface charge

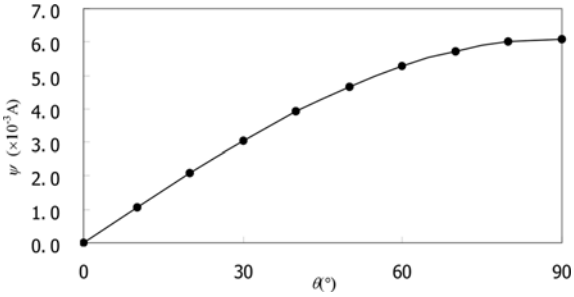

Fig. 8 Distribution of Ψ versus θ on the rim of the circular hole subjected to a sinusoidal surface charge

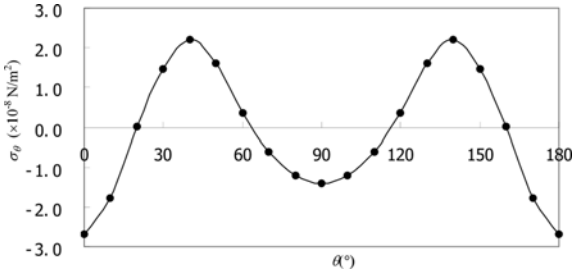

Fig. 9 Distribution of σ_θ versus θ on the rim of the circular hole subjected to a sinusoidal surface charge

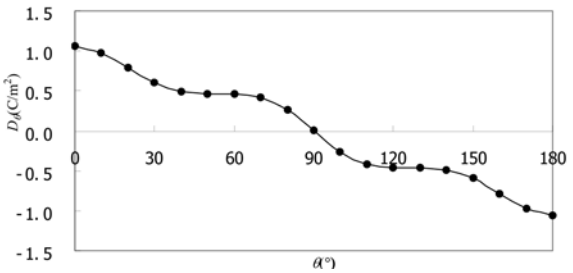

Fig. 10 Distribution of D_θ versus θ on the rim of the circular hole subjected to a sinusoidal surface charge

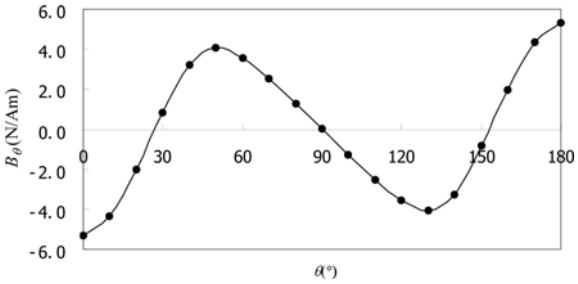

Fig. 11 Distribution of B_θ versus θ on the rim of the circular hole subjected to a sinusoidal surface charge

Example 4: Consider the plane problem of an infinite magnetoelectroelastic material with a circular hole, as shown in Fig. 12, respectively subjected to uniform distributed load $\sigma_z^\infty = \sigma_0$, electric displacement $D_z^\infty = D_0$ and magnetic induction $B_z^\infty = B_0$ on infinite, but no load on the rim of the hole. The radius of hole is still $r_0 = 1$ cm. The problem is treated as a plane-strain one, while the boundary condition at the rim of the hole as

$$\sigma_r = \tau_{r\theta} = D_r = B_r = 0 \qquad \text{at } r = r_0 \tag{28}$$

and the boundary condition on infinite as

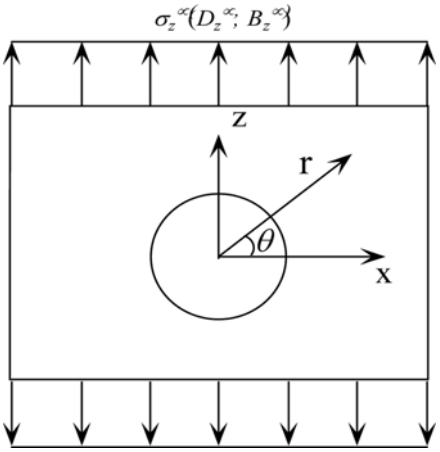

Fig. 12 A circular hole in an infinite plane magnetoelectroelastic solid

(a) under uniform distributed load σ_z^{∞}

$$\sigma_r(\theta) = \sigma_0 \sin^2\theta, \quad \tau_{r\theta}(\theta) = \sigma_0 \sin\theta\cos\theta, \quad D_r = B_r = 0 \quad \text{when} \quad r \to \infty \tag{29}$$

(b) under electric displacement D_z^{∞}

$$D_r(\theta) = D_0 \sin\theta, \quad D_\theta(\theta) = D_0 \cos\theta, \quad \sigma_r = B_r = 0 \quad \text{when} \quad r \to \infty \tag{30}$$

(c) magnetic induction B_z^{∞}

$$B_r(\theta) = B_0 \sin\theta, \quad B_\theta(\theta) = B_0 \cos\theta, \quad \sigma_r = D_r = 0 \quad \text{when} \quad r \to \infty \tag{31}$$

In the calculation, set the ratio of the virtual boundary and the real boundary as 0.7, take total 60 collocations on the virtual boundary and the real boundary, respectively. (Note: Presently no exact solution is found)

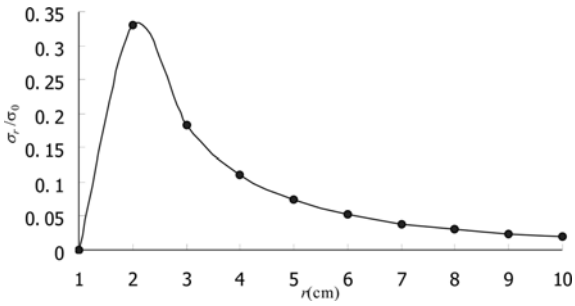

Fig. 13 The distribution of σ_r versus r when $\theta = 0$ and subjected to σ_z^{∞}

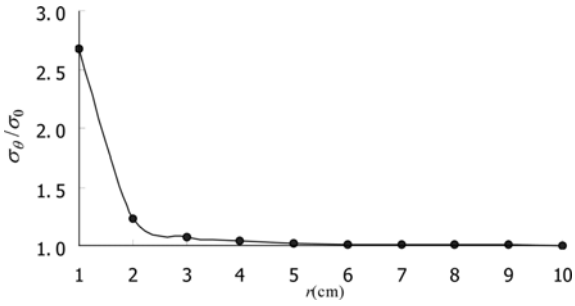

Fig. 14 The distribution of σ_θ versus r when $\theta = 0$ and subjected to σ_z^{∞}

Fig. 13 and Fig. 14 indicate the distribution of σ_r, σ_θ with increase of r when $\theta = 0$ due to σ_z^∞. As shown in Fig. 14, σ_θ is the maximum at rim of the hole and the stress concentration factor is 2.678. On infinite distance, both drive to single tension state, that is, $\sigma_r \to 0$, $\sigma_\theta \to \sigma_0$.

Fig. 15 and Fig. 16 indicate the distribution of σ_r, σ_θ with the increase of r when $\theta = \pi/2$ due to σ_z^∞. As shown in the Figs. 15-16, σ_r gradually rises with increase of r and finally approaches to σ_0; negative σ_θ exists on the region near the rim of the hole, but it quickly vanishes with the increase of r.

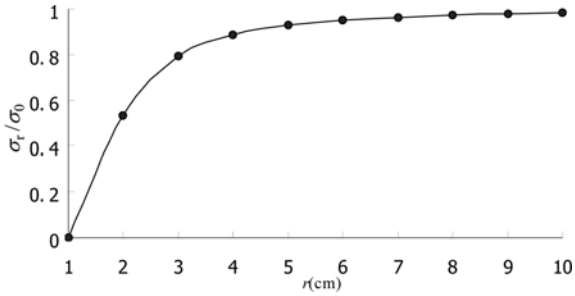

Fig. 15 The distribution of σ_r versus r when $\theta = \pi/2$ and subjected to σ_z^∞

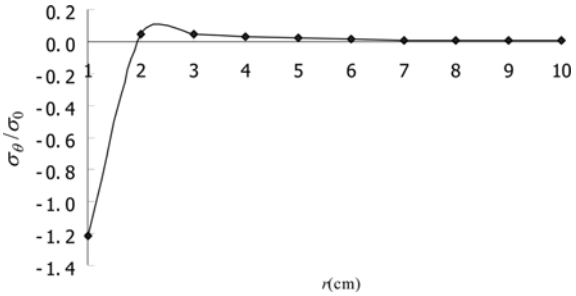

Fig. 16 The distribution of σ_θ versus r when $\theta = \pi/2$ and subjected to σ_z^∞

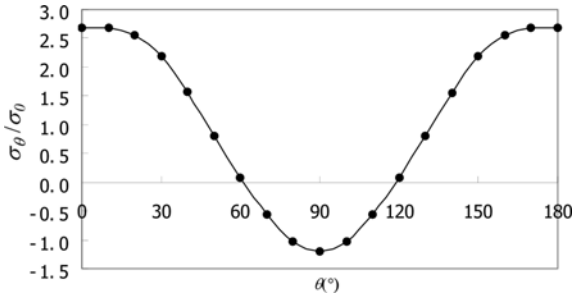

Fig. 17 Distribution of σ_θ versus θ on the rim of the circular hole subjected to σ_z^∞

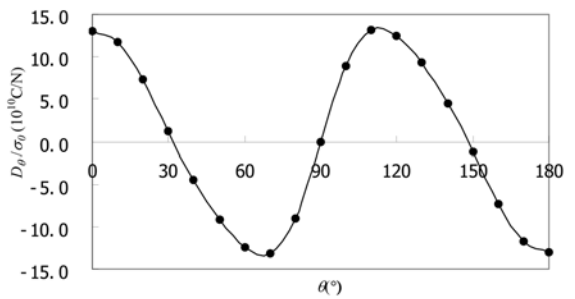

Fig. 18 Distribution of D_θ versus θ on the rim of the circular hole subjected to σ_z^∞

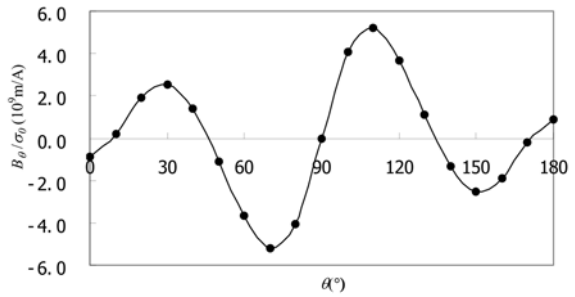

Fig. 19 Distribution of B_θ versus θ on the rim of the circular hole subjected to σ_z^∞

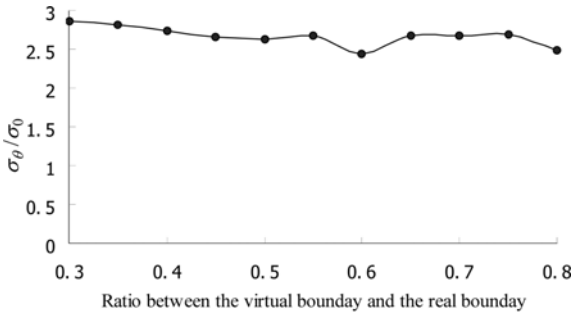

Fig. 20 The result of σ_θ at the point (1, 0) subjected to σ_z^∞, when the radius of the virtual boundary is given different values

Figs. 17-19 indicate the distribution of σ_θ, D_θ and B_θ at the rim of the hole due to σ_z^∞. The maximum values of σ_θ are observed at $\theta = 0^o$ and $\theta = 180^o$, whereas D_θ reaches its maximum value at $\theta = 65^o$ and $\theta = 115^o$, and B_θ reaches its maximum value at $\theta = 70^o$ and $\theta = 110^o$ as indicated in the Figs. 17-19.

Fig. 20 indicates numerical results with the different virtual boundary due to σ_z^∞. The figure shows that the perfect results can be obtained when take the virtual boundary in sizeable scopes. Here it must be explained that in a sense the virtual boundary element method approaches the conventional boundary element method when the virtual boundary approaches the real boundary,

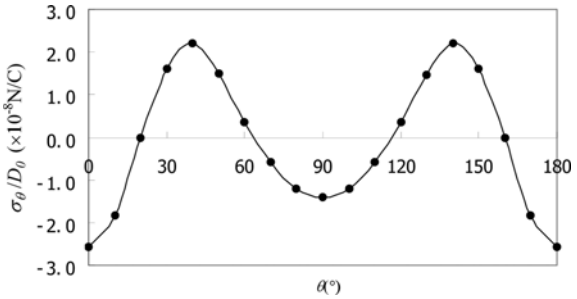

Fig. 21 Distribution of σ_θ versus θ on the rim of the circular hole subjected to D_z^∞

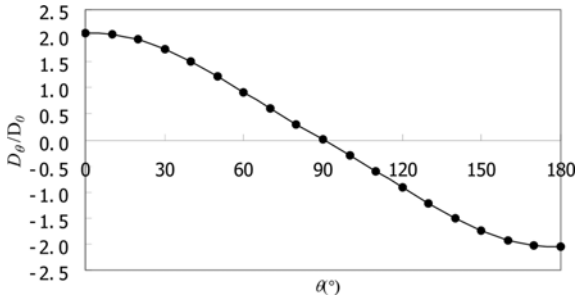

Fig. 22 Distribution of D_θ versus θ on the rim of the circular hole subjected to D_z^∞

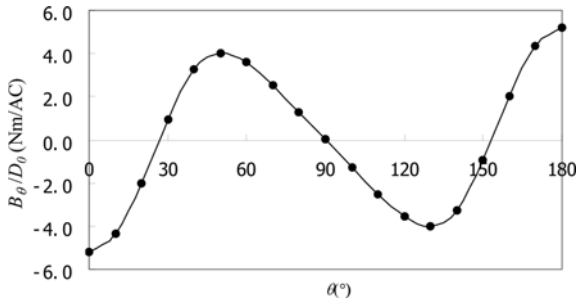

Fig. 23 Distribution of B_θ versus θ on the rim of the circular hole subjected to D_z^∞

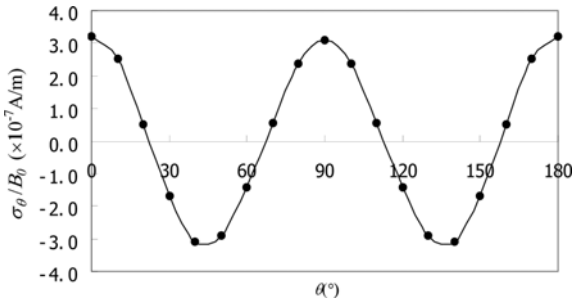

Fig. 24 Distribution of σ_θ versus θ on the rim of the circular hole subjected to B_z^∞

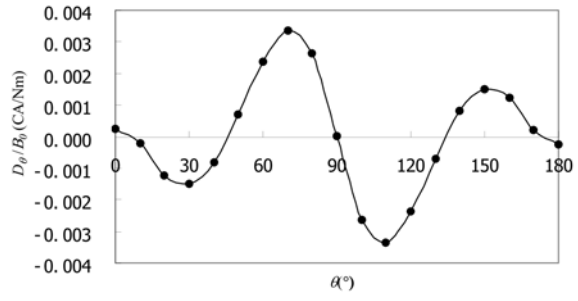

Fig. 25 Distribution of D_θ versus θ on the rim of the circular hole subjected to B_z^∞

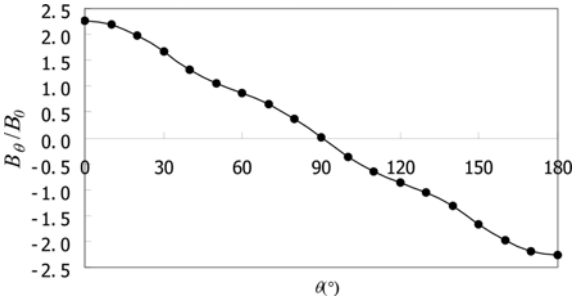

Fig. 26 Distribution of B_θ versus θ on the rim of the circular hole subjected to B_z^∞

that is, there are singular integral and major errors; on the other hand, that the smaller radius of virtual boundary leads to ill-conditioned coefficient matrix and bad computational accuracy.

Figs. 21-23 indicate the distribution of σ_θ, D_θ and B_θ at the rim of the hole due to D_z^∞. They all reach theirs maximum value at $\theta = 0^o$ and $\theta = 180^o$.

Figs. 24-26 indicate the distribution of σ_θ, D_θ and B_θ at the rim of the hole due to B_z^∞. The maximum values of σ_θ and B_θ are observed at $\theta = 0^o$ and $\theta = 180^o$, whereas D_θ reaches its maximum value at $\theta = 70^o$ and $\theta = 110^o$ as indicated in Figs. 24-26.

6. Conclusions

The paper proposes the virtual boundary element-equivalent collocation method for the plane problem of magnetoelectroelastic solids. The numerical results show that:

(1) The virtual boundary element method successfully avoids singular integral existed in classical boundary element method. There is higher accuracy not only in the domain but also on the boundary. The method is an efficient numerical approach for problem of magnetoelectroelastic solids.

(2) When virtual boundary is outside of the real boundary, the ratio between the virtual boundary and real boundary should be taken 1.5-3.5; otherwise the ratio should be taken 0.3-0.8.

(3) The virtual boundary method is comprehensible and legible, and is easy to implement by program.

The paper only presents pilot study to the virtual boundary element method applied to magnetoelectroelastic solids, and there is lots of work needed to be done in the further.

Acknowledgements

The work was supported by the National Natural Science Foundation of China (No. 10172021).

References

Buchanan, George R. (2004), "Layered versus multiphase magneto-electro-elastic composites", *Composites Part B: Engineering*, **35**(5), 413-420.

Chen, W. (2002), "High-order fundamental and general solutions of convection-diffusion equation and their applications with boundary particle method", *Engineering Analysis with Boundary Elements*, **26**(7), 571-575.

Chen, W. (2002), "Meshfree boundary particle method applied to Helmhotz problems", *Engineering Analysis with Boundary Elements*, **26**(7), 577-581.

Ding, Haojiang and Jiang, Aimin (2003), "The fundamental solutions for transversely isotropic magnetoelectroelastic media and boundary integral formulation", *Science in China* (series E), **33**(9), 845-855.

Ding, Haojiang and Jiang, Aimin (2004), "A boundary integral formulation and solution for 2D problem in magneto-electro-elastic media", *Comput. Struct.*, **82**(21-22), 1599-1607.

Garcia Lage, R. *et al.* (2004), "Layerwise partial mixed finite element analysis of magneto-electro-elastic plates", *Comput. Struct.*, **82**(17-19), 1293-1301.

Jiang, Aimin and Ding, Haojiang (2004), "Analytical solutions to magneto-electro-elastic beams", *Struct. Eng. Mech.*, **18**(2), 195-209.

Liu, Jinxi and Liu, Xianglin *et al.* (2001), "Green's functions for anisotropic magnetoelectroelastic solids with an

elliptical cavity or a crack", *Int. J. Eng. Sci.*, **39**(12), 1405-1418.
Mukhejee, S. and Chai, M.K. *et al.* (2000), "Evaluation of nearly singular integrals in boundary element coutour and node methods for three-dimensional linear elasticity", *Int. J. Solids Struct.*, **37**(51), 7633-7654.
Mukherjee, Y.X. and Mukherjee, S. (1997), "The boundary node method for potential problems", *Int. J. Numer. Meth. Eng.*, **40**(5), 797-815.
Pan, E. and Heyliger, P.R. (2003), "Exact solutions for magneto-electro-elastic laminates in cylindrical bending", *Int. J. Solids Struct.*, **40**(24), 6859-6876.
Sun, Huanchun and Yao, Weian (1997), "Virtual boundary element-linear complementary equations for solving the elastic obstacle problems of thin plate", *Finite Elements in Analysis and Design*, **27**(2), 153-161.
Sun, Huanchun and Zhang, Lizhou *et al.* (1999), *Nonsingularity Boundary Element Methods*, Dalian: Dalian University of Technology Press (in Chinese).
Wang, B.-L. and Mai, Y.-W. (2004), "Fracture of piezoelectromagnetic materials", *Mechanics Research Communications*, **31**(1), 65-73.
Wang, X. and Shen, Y.P. (2002), "The general solution of three-dimensional problems in magnetoelectroelastic media", *Int. J. Eng. Sci.*, **40**(10), 1069-1080.
Wang, X. and Shen, Y.P. (2003), "Inclusions of arbitrary shape in magnetoelectroelastic composite materials", *Int. J. Eng. Sci.*, **41**(1), 85-102.
Yao, Weian and Wang, Hui (2005), "Virtual boundary element integral method for 2-D piezoelectric media", *Finite Elements in Analysis and Design*, **41**(9-10), 875-891.